COMPACT RADIO SOURCES IN THE FIELD OF TYCHO'S SUPERNOVA REMNANT

Luis F. Rodríguez[1], Vanessa Yanza[1], and Sergio A. Dzib[2]

ABSTRACT

We present sensitive, high angular resolution Jansky Very Large Array observations made in 2014 at 1.50 GHz toward the field of Tycho's supernova remnant. We detect a total of 36 compact sources in a field with radius of 13 arcmin. This number is consistent with the expected number of background sources. We use older observations made with the classic Very Large Array to compare with the 2014 observations and search for sources showing large proper motions that could be related to the donor companion of the exploding white dwarf that produced the supernova in 1572. The comparison of the positions for the two sets of observations does not show sources with large proper motions and supports the conclusion that all sources detected are extragalactic and unrelated to the supernova field.

RESUMEN

Presentamos observaciones sensitivas de alta resolución angular hechas en 2014 con el Jansky Very Large Array a 1.50 GHz hacia el campo de la remanente de supernova de Tycho. Detectamos un total de 36 fuentes compactas en un campo con radio de 13 minutos de arco. Usamos observaciones más antiguas hechas con el VLA clásico para comparar con los datos de 2014 buscando fuentes con movimientos propios grandes que pudieran estar relacionadas con la compañera donante de la enana blanca que explotó y produjo la supernova en 1572. La comparación de posiciones entre los dos conjuntos de observaciones no revela fuentes con grandes movimientos propios y apoya la conclusión de que todas las fuentes detectadas son fuentes extragalácticas de fondo sin relación con el campo de la supernova.

Key Words: astrometry — ISM: supernova remnants — radio continuum: general — stars: general

1. INTRODUCTION

Tycho's 1572 supernova (SN 1572, 3C 10, B Cas) has been classified as a standard type Ia on the basis of its light-echo spectrum (Krause et al. 2008). This supernova type is very important since it is a cosmological standard candle that has allowed to determine the accelerated expansion history of the Universe (Riess et al. 1998; Perlmutter et al. 1999). It is produced by the thermonuclear explosion of a white dwarf accreting from a companion in a close binary system. In the most favored model the white dwarf is fully disrupted when it reaches the Chandrasekhar limit, leaving no collapsed object. The companion then leaves the original position of the binary with the orbital velocity it had at the moment of the explosion, that can be as large as ≈1,000 km s^{-1} (Geier et al. 2015). The nature of the companion is poorly understood, and it can be a main sequence, subgiant, red giant, AGB, He star or even another white dwarf (Iben 1997; Ruiz-Lapuente 2019).

The determination of the nature of the progenitor (the exploding star) of type Ia supernovae has been the subject of many studies (e.g. Maoz et al. 2014). Less effort has gone into understanding the surviving donor companion (e.g. Ruiz-Lapuente 2019). Only a handful of nearby type Ia supernova remnants (SNRs) have been inspected in search of the companion star (Pan et al. 2014). Importantly, the search for the binary companion of Tycho's SN 1572 has yielded a candidate: a G-type subgiant star labelled Tycho-G (Ruiz-Lapuente 2004; González-Hernández

---

[1]Instituto de Radioastronomía y Astrofísica, UNAM, México.

[2]Max-Planck-Institut für Radioastronomie, Germany.

2009). The star is relatively close to the center of the supernova remnant, its distance is compatible with it being inside the SNR, it has significantly higher radial velocity and proper motions than other stars at the same location in the Galaxy, and it shows signs of pollution from the supernova ejecta. However, other studies have questioned Tycho-G as the companion donor star because they do not find the expected large stellar rotation (Kerzendorf et al. 2009), they do not confirm the unusual chemistry (Kerzendorf et al. 2013), or their proposed explosion center does not overlap with the past stellar position at the time of the explosion (Xue & Schaefer 2015; Millard et al. 2022). An additional problem is that the Gaia DR3 (Gaia collaboration et al. 2016; 2022) distance of Tycho-G (Gaia DR3 431160359413315328 in the Gaia designation) is $1.93^{+0.45}_{-0.31}$ kpc while the distance to the supernova is 2.8 ± 0.4 kpc (Kozlova & Blinnikov 2018). Then, the ±1-σ error bars fall close but do not overlap. More accurate distances could help solve this problem.

The lack of clearly confirmed donor companion stars in type Ia SNRs (Schaefer & Pagnotta 2012; González Hernández et al. 2012; Di Stefano & Kilic 2012; Pan et al. 2014; Ruiz-Lapuente et al. 2018) has led to a questioning of the favored 'single-degenerate' path (mass transfer from a normal companion star to a ultimately exploding white dwarf) in favor of the 'double-degenerate' scenario, in which the merger of two white dwarfs produces an explosion that leaves no stellar remnant.

The field of Tycho's SNR has been studied in radio with emphasis on the morphology and proper motions of the extended synchrotron shell (Dickel et al. 1991; Reynoso et al. 1997; Williams et al. 2016). In this paper we present a study of the compact (taken to be $\leq 6''$) radio sources in this field to search for a source with large proper motion that could be related to the companion star. Stars of low optical luminosity on the main sequence are very rarely detected in radio (Kimball et al. 2009). As noted by Gaidos et al. (2000), the radio emission of normal, single solar analogs rapidly declines to undetectable levels after a few hundred million years. On the other hand, it is known that rotation is the main agent responsible for the level of magnetic activity in cool stars (Güdel 2002). Large magnetic fields facilitate the production of radio emission via mechanisms such as gyrosynchrotron. The possible relation between rotation and radio emission is supported by the study of McLean et al. (2012) who find that rapidly rotating ($v \sin i \geq 20$ km s^{-1}) ultracool dwarfs have a higher radio detection frac-

tion by about a factor of three compared to objects with $v \sin i \leq 10$ km s^{-1}. Also, Lim & White (1995) detected at 3.6 cm three of the four ultrafast ($v \sin i \geq 30$ km s^{-1}) rotators in the Pleiades. The justification for our search is that the companion donor stars are expected to have large rotation velocities ($v \geq 20$ km s^{-1} for a donor mass ≥ 0.2 $M_\odot$; Kerzendorf et al. 2009) that could enhance their radio emission. It should be pointed out, however, that there are a variety of mechanisms that can produce detectable radio emission in stars (Güdel 2002; Dzib et al. 2013). In § 2 we present the observations, while in § 3 we discuss some individual sources. Finally, in § 4 we present our conclusions.

2. OBSERVATIONS

2.1. *1.50 GHz Observations for Epoch 2014 February 20*

The main set of data used in this paper corresponds to observations made with the Karl G. Jansky Very Large Array (VLA) of NRAO[3] in the A configuration on 2014 February 20 (2014.140). The observations were taken under project 13A-426 in the L-band (0.96-1.97 GHz) using 16 spectral windows, each 64 MHz wide. The amplitude calibrator was J0137+3309 (3C48) and the gain calibrator was J0217+7349. The phase center of the observations was at $RA(J2000) = 00^h 25^m 18\overset{s}{.}966$; $DEC(J2000) = 64° 08' 20\overset{''}{.}41$. The data were edited and calibrated following the standard procedures inside the CASA (Common Astronomy Software Applications; McMullin et al. 2007) package of NRAO and the pipeline provided for VLA[4] observations.

We made images using a robust weighting (Briggs 1995) of 0 and visibilities with baselines larger than 6 kλ, to suppress structures larger than ≈ 30 arcsec. The final image had an rms noise of 28 μJy beam^{-1} at the phase center and a synthesized beam of $1\overset{''}{.}44 \times 0\overset{''}{.}83$; PA $= -88°$. The images were corrected for the primary beam response. The images were also corrected for wide-field effects using the gridding option *widefield* with 10×10 subregions in the task TCLEAN. A region with a radius of 13 arcmin was inspected for sources with peak emission above 6-σ (168 μJy beam^{-1}). We detected a total of 36 sources. Their positions, flux densities, spectral indices, angular sizes and counterparts, when found, are given in

---

[3]The National Radio Astronomy Observatory is a facility of the National Science Foundation operated under cooperative agreement by Associated Universities, Inc.

[4]https://science.nrao.edu/facilities/vla/data-processing/pipeline.

Table 1. The positions and flux densities were determined using the task IMFIT of CASA. The spectral indices were determined by splitting the total bandwidth in four bandwidths of 256 MHz each, making images and fitting the four flux densities obtained for each source as a function of frequency with a linear regression in the log-log plane.

Following the procedure of Anglada et al. (1998) we determine that 37±6 background sources were expected. This estimate suggests that most, and probably all, of the sources detected are background objects unrelated to the remnant region. Nevertheless, within the uncertainty, it cannot be ruled out that a few sources could be associated with the remnant.

2.2. *Observations with the Classic VLA*

To gain information on the time variability and possible proper motions of the sources found in the 2014 image, we analyzed classic VLA observations made in the A configuration on the three epochs listed in Table 2. As in the 2014 data, the amplitude calibrator was J0137+3309 (3C48) and the gain calibrator was J0217+7349 for the three epochs. The data were concatenated to gain signal to noise ratio and assigned an average epoch of 1993.468 and an average frequency of 1.43 GHz. The data were edited and calibrated using the software package Astronomical Image Processing System (AIPS) of NRAO. We made images using a robust weighting (Briggs 1995) of 0 and visibilities with baselines larger than 6 kλ, to suppress structures larger than $\approx$30 arcsec.

The final image had an rms noise of 75 μJy beam^{-1} at the phase center and a synthesized beam of $1''39 \times 1''33$; PA = +28°. As for the 2014 image, a region with radius of 13 arcmin was inspected for sources with peak emission above 6-σ (450 μJy beam^{-1}). We detected a total of 17 sources. Again, following the procedure of Anglada et al. (1998) we determined that 18±4 background sources were expected. As in the more sensitive 2014 data, this estimate suggests that most, and probably all, of the sources detected are background objects unrelated to the remnant region. Their positions and flux densities are given in Table 3. In this Table we also list the difference in RA and DEC between the 2014 positions and those obtained from the classic VLA data.

All 17 sources detected in the image from the classic VLA data were detected in the more sensitive (by a factor of 2.7) 2014 observations. To compare the flux densities at the two epochs we corrected the 2014 flux densities from 1.50 to 1.43 GHz using the spectral indices listed in Table 1. This correction is small, of order 5-10%. In the last column of Table 3 we list the ratio of the flux densities. Eight of the 17 sources have a ratio consistent within noise with 1 and thus no variability. Only source 6 shows a variability larger than a factor of 2, decreasing by a factor of 4 between databases.

2.3. *Upper Limits to the Proper Motions*

Analyzing Table 3 we find that the position differences between the 2014 image and the classic VLA image (Columns 5 and 6) are above a conservative 5-σ value only for sources 19, 31, 34 and 35. Should these possible small proper motions be considered as real? Sources 31, 34 and 35 are resolved angularly (see Table 1) and this characteristic could well account for the small difference in position between epochs due to differences in the beam shape. The position differences for the remaining source 19 are of order of only $\approx 0''1$. Taking this displacement as an upper limit to the true proper motions, we can crudely set an upper limit to the velocity of the sources in the plane of the sky. Given the time interval of 20.672 yr between the two datasets and a distance of 2.8 kpc to the supernova (Kozlova & Blinnikov 2018) this results in an upper limit of 65 km s^{-1} for the velocity of the radio sources in the plane of the sky, if they were located at the distance of the supernova. As noted before, it is most probable that all sources are extragalactic and that the small position differences measured are the result of noise and not true displacements. Supporting the extragalactic interpretation is the fact that none of the 36 radio sources has a counterpart in the Gaia DR3 catalog (Gaia collaboration et al. 2016; 2022). Tycho's SNR is almost in the plane of the Galaxy (it has a galactic latitude of 1°4). Then, extragalactic objects in this direction will be heavily obscured in the optical and very difficult to detect in the observations of the Gaia project.

2.4. *The Non Detection of Tycho-B*

The star Tycho-G was not detected in our observations. Perhaps more interestingly, the star Tycho-B was not detected either. Tycho-B is a fast-rotator A-type star that has been proposed as a candidate to be the donor companion of the exploding white dwarf that produced SN 1572 (Kerzendorf et al. 2013), although this proposal has been questioned later (Kerzendorf et al. 2018).

The best studied case of radio emission from a rapidly rotating A-type star is that of Altair (α Aql; White et al. 2021). From the model of these authors we estimate that Altair is expected to have

TABLE 1

PARAMETERS OF COMPACT RADIO SOURCES AT 1.50 GHZ (2014 FEBRUARY 20)

No.	Position[a] RA(J2000)	DEC(J2000)	Flux Density(μJy)	Spectral Index	Angular Dimensions[b] ($\theta_{maj} \times \theta_{min}$; PA)	Counterpart
1	00 23 16.800±0.007	64 20 25.46±0.03	1808±200	+0.00±0.52	$1.4 \pm 0.2 \times 0.9 \pm 0.3$; 31 ± 25	$\cdots$
2	00 23 24.220±0.010	63 59 07.43±0.02	840±95	−1.35±0.45	≤ 0.5	$\cdots$
3	00 23 30.774±0.013	64 08 04.34±0.05	528±75	−1.14±0.48	≤ 0.5	$\cdots$
4	00 23 40.826±0.011	64 10 52.87±0.03	416±46	−1.45±0.47	≤ 0.5	$\cdots$
5	00 24 11.264±0.007	64 09 50.02±0.01	521±31	−0.04±0.30	≤ 0.5	$\cdots$
6	00 24 18.177±0.012	63 58 58.03±0.12	429±62	+0.02±0.54	≤ 0.5	$\cdots$
7	00 24 30.749±0.009	64 02 00.33±0.03	348±44	−0.59±0.54	≤ 0.5	$\cdots$
8	00 24 39.839±0.013	64 01 05.93±0.05	381±51	−1.31±0.53	≤ 0.5	$\cdots$
9	00 24 41.071±0.006	64 03 56.91±0.01	596±37	+0.03±0.30	≤ 0.5	$\cdots$
10	00 24 44.695±0.006	64 04 53.40±0.05	561±51	−1.63±0.42	≤ 0.5	$\cdots$
11	00 24 46.084±0.006	64 12 36.46±0.02	528±37	−1.27±0.34	≤ 0.5	$\cdots$
12	00 24 51.749±0.006	63 59 08.33±0.02	601±55	−0.89±0.42	≤ 0.5	$\cdots$
13	00 24 56.742±0.007	64 17 50.66±0.03	607±44	−1.69±0.34	≤ 0.5	$\cdots$
14	00 24 58.631±0.009	64 10 56.82±0.03	486±53	−1.03±0.37	≤ 0.5	$\cdots$
15	00 25 01.637±0.005	64 07 47.75±0.01	843±46	−1.49±0.20	≤ 0.5	$\cdots$
16	00 25 10.166±0.003	64 16 28.06±0.01	1258±53	−0.64±0.20	≤ 0.5	$\cdots$
17	00 25 14.131±0.027	64 00 15.08±0.12	1652±288	−1.98±0.61	$4.8 \pm 1.1 \times 2.2 \pm 0.7$; 45 ± 14	$\cdots$
18	00 25 16.087±0.016	63 59 40.96±0.14	796±108	−0.99±0.63	$2.3 \pm 0.5 \times 1.3 \pm 0.5$; 168 ± 27	$\cdots$
19	00 25 19.270±0.001	64 08 53.28±0.01	5150±68	−1.30±0.06	≤ 0.5	[RMG97] 002231.23+635216.9
20	00 25 26.037±0.002	64 04 40.89±0.01	3575±90	−1.11±0.08	≤ 0.5	[RMG97] 002237.96+634804.7
21	00 25 34.981±0.004	64 08 43.06±0.01	741±33	−0.70±0.27	≤ 0.5	$\cdots$
22	00 25 36.024±0.007	64 10 39.81±0.01	330±33	−1.31±0.52	≤ 0.5	$\cdots$
23	00 25 40.204±0.005	64 13 05.95±0.01	537±40	−0.10±0.35	≤ 0.5	$\cdots$
24	00 25 40.601±0.006	64 11 33.72±0.02	607±53	−0.92±0.33	≤ 0.5	$\cdots$
25	00 25 50.714±0.022	64 09 28.82±0.17	1058±115	−0.95±0.49	$4.6 \pm 0.7 \times 2.3 \pm 0.5$; 7 ± 11	Nucleus of radio galaxy
26	00 26 05.112±0.002	64 17 13.89±0.01	2306±81	−0.93±0.14	≤ 0.5	$\cdots$
27	00 26 08.967±0.006	64 16 33.89±0.02	590±51	−0.98±0.36	≤ 0.5	$\cdots$
28	00 26 16.279±0.014	64 21 33.46±0.14	3476±209	−1.60±0.40	$5.7 \pm 0.6 \times 1.2 \pm 0.3$; 29 ± 3	Disk galaxy 2MFGC 305
29	00 26 23.102±0.007	64 12 32.06±0.01	581±35	−1.61±0.35	≤ 0.5	$\cdots$
30	00 26 23.656±0.010	64 04 42.34±0.04	253±46	−1.33±0.55	≤ 0.5	$\cdots$
31	00 26 24.059±0.003	63 56 24.03±0.01	1725±123	−0.30±0.32	$1.0 \pm 0.1 \times 0.6 \pm 0.3$; 0 ± 17	$\cdots$
32	00 26 28.133±0.012	63 58 36.78±0.08	508±62	+1.05±0.39	≤ 0.5	$\cdots$
33	00 26 30.651±0.017	64 14 36.13±0.06	352±57	+0.49±0.62	≤ 0.5	$\cdots$
34	00 26 50.729±0.002	64 10 25.52±0.01	3324±112	−1.01±0.14	$1.0 \pm 0.1 \times 0.6 \pm 0.1$; 62 ± 7	$\cdots$
35	00 26 51.389±0.002	64 02 20.16±0.01	20284±682	−0.99±0.11	$1.3 \pm 0.1 \times 0.8 \pm 0.1$; 69 ± 1	Radio source EQ 0024+638
36	00 27 11.599±0.017	64 12 44.78±0.02	462±73	+0.25±0.55	≤ 0.5	$\cdots$

[a]Right ascension (RA) is given in hours, minutes, and seconds. Declination (DEC) is given in degrees, arcminutes, and arcseconds.

[b]The deconvolved major (θ_{maj}) and minor (θ_{min}) axes are given in arcsec. The position angle (PA) is given in degrees.

TABLE 2

OBSERVATIONS WITH THE CLASSIC VLA IN A CONFIGURATION

Project	Epoch	Amplitude Calibrator	Gain Calibrator	Frequency (GHz)	Bandwidth (MHz)
AV84	1983 Nov 13 (1983.868)	J0137+3309	J0217+7349	1.38	6.25
AM437	1994 Mar 18 (1994.211)	J0137+3309	J0217+7349	1.51	6.25
AR464	2002 Apr 29 (2002.326)	J0137+3309	J0217+7349	1.41	6.25

a flux density of $\simeq$ 10 μJy at the frequency of 1.5 GHz. Tycho-B, with position $RA(J2000) = 00^h\ 25^m\ 19\overset{s}{.}985$; $DEC(J2000) = +64° \ 08'17\overset{''}{.}19$, is located at a distance of 2.7 kpc (Gaia Collaboration 2020). On the other hand, Altair is located at a distance of only 5.1 pc (van Leeuwen 2007). We then conclude that if Tycho-B had a similar radio emission to that of Altair, its flux density would be $(2700/5.1)^2 = 2.8 \times 10^5$ weaker and undetectable with present instrumentation.

TABLE 3

PARAMETERS OF COMPACT RADIO SOURCES FROM CLASSIC VLA DATA

	Position[a]		Flux	ΔRA[b]	ΔDEC[b]	Flux Ratio
No.	RA(J2000)	DEC(J2000)	Density(μJy)	(seconds)	(arcseconds)	(2014/1983)
6	00 24 18.052±0.099	63 58 58.73±1.02	1903±414	0.125±0.099	-0.70±1.03	0.23±0.06
9	00 24 41.071±0.014	64 03 56.99±0.09	663±163	0.000±0.015	-0.08±0.09	0.90±0.23
10	00 24 44.701±0.013	64 04 53.39±0.15	692±182	-0.006± 0.010	0.01±0.16	0.87±0.24
12	00 24 51.749±0.016	63 59 07.99±0.17	815±107	0.000±0.017	0.34±0.17	0.77±0.12
13	00 24 56.718±0.023	64 17 50.48±0.16	582±193	0.024±0.024	0.18±0.16	1.13±0.38
15	00 25 01.648±0.009	64 07 47.89±0.07	1130±179	-0.011±0.010	-0.14±0.07	0.80 ±0.13
16	00 25 10.161±0.008	64 16 27.85±0.06	1735±197	0.005±0.009	0.21±0.06	0.75±0.09
17	00 25 14.076±0.097	64 00 13.84±0.69	3782±530	0.055± 0.101	1.24±0.70	0.48±0.11
19	00 25 19.282±0.001	64 08 53.40±0.01	6657±166	-0.012±0.001	-0.12±0.01	0.82±0.02
20	00 25 26.046±0.002	64 04 40.97±0.02	3831±168	-0.010±0.003	-0.08±0.02	0.98 ±0.05
21	00 25 34.987±0.011	64 08 43.23±0.07	974±173	-0.006±0.012	-0.17± 0.07	0.79±0.14
24	00 25 40.605±0.017	64 11 34.00±0.11	675±176	-0.004±0.018	-0.28±0.11	0.94± 0.26
26	00 26 05.110±0.009	64 17 13.62±0.05	2229±216	0.002±0.009	0.27±0.06	1.08±0.11
28	00 26 16.278±0.053	64 21 32.73±0.35	6157±1010	0.012±0.055	0.57±0.37	0.61±0.11
31	00 26 24.054±0.014	63 56 23.45±0.07	1338±214	0.005± 0.014	0.58± 0.07	1.31±0.23
34	00 26 50.724±0.005	64 10 25.28±0.03	3564±222	0.005±0.005	0.24±0.03	0.98±0.08
35	00 26 51.364±0.002	64 02 19.78±0.01	20092±263	0.025±0.003	0.38±0.01	1.06±0.04

[a]Right ascension (RA) is given in hours, minutes, and seconds. Declination (DEC) is given in degrees, arcminutes, and arcseconds.

[b]Position differences given by 2014 positions minus classic VLA positions.

3. INDIVIDUAL SOURCES

To gain information on the sources detected we used the SIMBAD database to search for counterparts within a few arcsec of the radio position.

3.1. *Sources 19 and 20*

These sources are reported by Reynoso et al. (1997) in their study of the expansion of the supernova remnant. They used them to align their images at different epochs. Their compact size and negative spectral index (see Table 1) suggest they are background active galactic nuclei.

3.2. *Source 25*

This source seems to be the nucleus of a radio galaxy (see Figure 1). The lobes of the radio galaxy extend over $\approx 35''$ in the north-south direction. Since they are clearly extended, the lobes are not reported in our list of compact sources. The nucleus is elongated along the axis defined by the radio lobes and probably traces more recent ejections.

3.3. *Source 28*

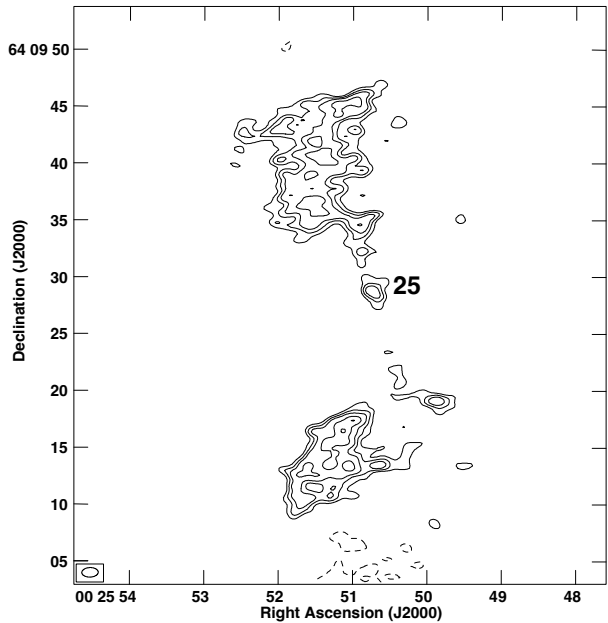This source was initially catalogued in the 2MASS-selected Flat Galaxy Catalog (2MFGC;

Fig. 1. Radio galaxy related to source 25. Contours are -4, 4, 5, 6, 8 and 10 times 17 μJy beam^{-1}, the rms noise of this region of the image. The synthesized beam ($1.''44 \times 0.''83$; $-88°$) is shown in the bottom left corner.
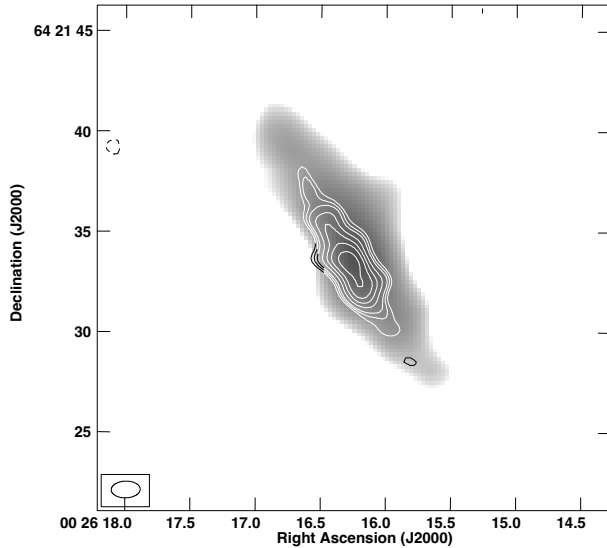
Fig. 2. The radio source 28 is shown in white contours
in this image. The contours are -4, 4, 5, 6, 8, 10, 12 and
15 times 11 μJy beam^{-1}, the rms noise of this region of
the image. The synthesized beam ($1.''44 \times 0.''83; -88°$)
is shown in the bottom left corner. The infrared image
from the Two Micron All Sky Survey (2MASS) in the K$_s$
band is shown in greyscale.

Mitronova et al. 2006). The sources in this cata-
log are expected to be disk galaxies selected from the
Extended Source Catalog of the Two Micron All-Sky
Survey (XSC 2MASS; Jarrett et al. 2000) on the ba-
sis of their 2MASS axial ratio being $a/b \geq 3$. We find
that the infrared and radio images approximately co-
incide and show similar elongated morphology (Fig-
ure 2).

3.4. Source 32

This source is interesting because it shows a
clearly positive spectral index (+1.05±0.39; Ta-
ble 1). All other sources in Table 1 have spectral
indices that are consistent within noise with a neg-
ative spectral index. Background radio sources usu-
ally show clearly negative spectral indices, taken to
be indicative of optically-thin synchrotron emission.
For example, Smolčić et al. (2016) obtained accurate
spectral indices for 159 sources by combining Aus-
tralia Telescope Compact Array (ATCA) 2.1 GHz
observations with Sydney University Molonglo Sky
Survey (SUMSS) 843 MHz data. Only three of the
sources show positive spectral indices ($\alpha > 0$).

Source 32 could be a high frequency peaker
(HFP). These are compact, sometimes powerful ex-
tragalactic radio sources with well-defined peaks in
their radio spectra above a few GHz, with most of
them being high redshift quasars (Dallacasa et al.

2000). A possible explanation for the HFP radio
sources is that we are observing synchrotron emis-
sion produced by blazars caught during a flare, when
a highly self-absorbed (optically-thick) component
dominates the emission (Tinti et al. 2005)

3.5. Source 35

This is the brightest compact source in the region
considered. It was reported previously by Schwarz et
al. (1995) from HI VLA observations made in 1993
in the C configuration. These authors proposed that
it is a background source. It is an elongated source
(see Table 1) and it could be a disk galaxy seen edge-
on or an unresolved radio galaxy.

4. CONCLUSIONS

Our main conclusions are the following:
(1) We compared observations made in the
L-band toward the Tycho supernova remnant in 2014
with the Jansky VLA and previously with the clas-
sic VLA. The purpose of this comparison was to
search for radio sources showing large proper mo-
tions that could be related to the donor companion
of the exploding white dwarf that produced the su-
pernova in 1572. We failed to find radio sources with
large proper motions (≥ 65 km s^{-1}) and conclude
that most, and probably all, of the sources detected
are background extragalactic objects. However, we
argue that these donor companions could be radio
sources and believe that its search in other Type Ia
supernova remnants is worthwhile.

(2) We discussed several sources individually and
concluded that their characteristics are compatible
with them being most likely background extragalac-
tic sources. Source 28 is most probably a disk galaxy
seen edge-on. Source 32 could be a high frequency
peaker, possibly a blazar caught during a flare.

This publication makes use of data products from
the Two Micron All Sky Survey, which is a joint
project of the University of Massachusetts and the
Infrared Processing and Analysis Center, funded by
the National Aeronautics and Space Administration
and the National Science Foundation. This research
has made use of the SIMBAD database, operated at
CDS, Strasbourg, France.

REFERENCES

Anglada, G., Villuendas, E., Estalella, R., et al. 1998,
   AJ, 116, 2953, https://doi.org/10.1086/300637
Bridle, A. H. & Schwab, F. R. 1999, ASPC 180, Synthesis
   Imaging in Radio Astronomy II, ed. G. B. Taylor, C.
   L. Carilli, and R. A. Perley, 371

Briggs, D. S. 1995, AAS, 187, 11202

Dallacasa, D., Stanghellini, C., Centonza, M., & Fanti, R. 2000, A&A, 363, 887, https://doi.org/10.48550/arXiv.astro-ph/0012428

Dickel, J. R., van Breugel, W. J. M., & Strom, R. G. 1991, AJ, 101, 2151, https://doi.org/10.1086/115837

Di Stefano, R. & Kilic, M. 2012, ApJ, 759, 56, https://doi.org/10.1088/0004-637X/759/1/56

Dzib, S. A., Rodríguez, L. F., Loinard, L., et al. 2013, ApJ, 763, 139, https://doi.org/10.1088/0004-637X/763/2/139

Gaia Collaboration, Prusti, T., de Bruijne, J. H. J., et al. 2016, A&A, 595, 1, https://doi.org/10.1051/0004-6361/201629272

Gaia Collaboration 2020, VizieR Online Data Catalog, I/350, https://doi.org/10.26093/cds/vizier.1350

Gaia Collaboration, Vallenari, A., Brown, A. G. A., et al. 2022, arXiv:2208.00211, https://doi.org/10.48550/arXiv.2208.00211

Gaidos, E. J., Güdel, M., & Blake, G. A. 2000, Geophys. Res. Lett., 27, 501, https://doi.org/10.1029/1999GL010740

Geier, S., Fürst, F., Ziegerer, E., et al. 2015, Sci, 347, 1126, https://doi.org/10.1126/science.1259063

González Hernández, J. I., Ruiz-Lapuente, P., Filippenko, A. V., et al. 2009, ApJ, 691, 1, https://doi.org/10.1088/0004-637X/691/1/1

González Hernández, J. I., Ruiz-Lapuente, P., Tabernero, H. M., et al. 2012, Nat, 489, 533, https://doi.org/10.1038/nature11447

Güdel, M. 2002, ARA&A, 40, 217, https://doi.org/10.1146/annurev.astro.40.060401.093806

Iben, I. 1997, Thermonuclear Supernovae, 486, 111, https://doi.org/10.1007/978-94-011-5710-0_8

Jarrett, T. H., Chester, T., Cutri, R., et al. 2000, AJ, 119, 2498, https://doi.org/10.1086/301330

Kerzendorf, W. E., Schmidt, B. P., Asplund, M., et al. 2009, ApJ, 701, 1665, https://doi.org/10.1088/0004-637X/701/2/1665

Kerzendorf, W. E., Yong, D., Schmidt, B. P., et al. 2013, ApJ, 774, 99, https://doi.org/10.1088/0004-637X/774/2/99

Kerzendorf, W. E., Long, K. S., Winkler, P. F., et al. 2018, MNRAS, 479, 5696, https://doi.org/10.1093/mnras/sty1863

Kimball, A. E., Knapp, G. R., Ivezić, Ž., et al. 2009, ApJ, 701, 535, https://doi.org/10.1088/0004-637X/701/1/535

Kozlova, A. V. & Blinnikov, S. I. 2018, Journal of Physics Conference Series, 1038, 012006, https://doi.org/10.1088/1742-6596/1038/1/012006

Krause, O., Tanaka, M., Usuda, T., et al. 2008, Nature, 456, 617, https://doi.org/10.1038/nature07608

Lim, J. & White, S. M. 1995, ApJ, 453, 207, https://doi.org/10.1086/176380

Maoz, D., Mannucci, F., & Nelemans, G. 2014, ARA&A, 52, 107, https://doi.org/10.1146/annurev-astro-082812-141031

McLean, M., Berger, E., & Reiners, A. 2012, ApJ, 746, 23, https://doi.org/10.1088/0004-637X/746/1/23

McMullin, J. P., Waters, B., Schiebel, D., et al. 2007, ASPC 376, Astronomical Data Analysis Software and Systems, ed. R. A. Shaw, F. Hill, & J. Bell (Tuczon, AZ: ASPC), 127

Millard, M. J., Park, S., Sato, T., et al. 2022, ApJ, 937, 121, https://doi.org/10.3847/1538-4357/ac8f30

Mitronova, S. N., Karachentsev, I. D., Karachentseva, V. E., Jarett, T. H., & Kudrya, Y. N. 2006, VizieR Online Data Catalog (other), 0110, J/other/BSAO/57

Pan, K.-C., Ricker, P. M., & Taam, R. E. 2014, ApJ, 792, 71, https://doi.org/10.1088/0004-637X/792/1/71

Perlmutter, S., Aldering, G., Goldhaber, G., et al. 1999, ApJ, 517, 565, https://doi.org/10.1086/307221

Reynoso, E. M., Moffett, D. A., Goss, W. M., et al. 1997, ApJ, 491, 816, https://doi.org/10.1086/304997

Riess, A. G., Filippenko, A. V., Challis, P., et al. 1998, AJ, 116, 1009, https://doi.org/10.1086/300499

Ruiz-Lapuente, P., Comeron, F., Méndez, J., et al. 2004, Nature, 431, 1069, https://doi.org/10.1038/nature03006

Ruiz-Lapuente, P., Damiani, F., Bedin, L., et al. 2018, ApJ, 862, 124, https://doi.org/10.3847/1538-4357/aac9c4

Ruiz-Lapuente, P. 2019, NewAR, 85, 101523, https://doi.org/10.1016/j.newar.2019.101523

Schwarz, U. J., Goss, W. M., Kalberla, P. M., & Bengali, P. 1995, A&A, 299, 193

Schaefer, B. E. & Pagnotta, A. 2012, Nature, 481, 164, https://doi.org/10.1038/nature10692

Smolčić, V., Delhaize, J., Huynh, M., et al. 2016, A&A, 592, 10, https://doi.org/10.1051/0004-6361/201526818

Tinti, S., Dallacasa, D., de Zotti, G., Celotti, A., & Stanghellini, C. 2005, A&A, 432, 31, https://doi.org/10.1051/0004-6361:20041620

van Leeuwen, F. 2007, A&A, 474, 653, https://doi.org/10.1051/0004-6361:20078357

White, J. A., Tapia-Vázquez, F., Hughes, A. G., et al. 2021, ApJ, 912, 5, https://doi.org/10.3847/2041-8213/abf6da

Williams, B. J., Chomiuk, L., Hewitt, J. W., et al. 2016, ApJ, 823, 32, https://doi.org/10.3847/2041-8205/823/2/L32

Xue, Z. & Schaefer, B. E. 2015, ApJ, 809, 183, https://doi.org/10.1088/0004-637X/809/2/183

Sergio A. Dzib: Max-Planck-Institut für Radioastronomie, Auf dem Hügel 69, D-53121 Bonn, Germany.

Luis F. Rodríguez and Vanessa Yanza: Instituto de Radioastronomía y Astrofísica, Universidad Nacional Autónoma de México, Apartado Postal 3–72, 58090 Morelia, Michoacán, México (l.rodriguez@irya.unam.mx).